

Kinetically engendered sub-spinodal lengthscales in spontaneous dewetting of thin liquid films.

TirumalaRao Kotni, Jayati Sarkar,* and Rajesh Khanna†

Department of Chemical Engineering, Indian Institute of Technology Delhi, New Delhi-110016

(Dated: February 28, 2022)

Numerical simulations of spontaneous dewetting of non-slipping, variable viscosity unstable thin liquid films on homogeneous substrates reveal the existence of sub-spinodal lengthscales through formation of satellite holes, a marker of nucleated dewetting and/or heterogeneous substrates, in the late stages of dewetting if the liquid viscosity decreases continually with decreasing film thickness. These films also show established signatures of slipping films such as faster rupture and flatter morphologies in the early stages even without invoking any slippage.

PACS numbers: 68.15.+e, 47.20.Ma, 47.54.-r, 68.55.J-

Spontaneous dewetting of supported thin liquid films [1–4] is increasingly being harnessed to create template-free meso-nano patterned surfaces which find use in MEMS/NEMS, microfluidic devices, optoelectronic devices, anti-reflective coatings etc., [5]. As is the case, the lengthscales thus achieved are upper-bounded by a spinodal lengthscale which depends on the film thickness and liquid properties such as Hamaker Constants, hydrodynamic slippage at the solid interface, surface tension and mass density but is surprisingly independent of the elastic moduli [6–9]. To achieve smaller lengthscales one has to necessarily rely on nucleated dewetting (through distribution of nucleating sites) [10] and/or heterogeneity of the underlying solid substrate (due to formation of satellite holes around already growing holes) [11]. Thus, being able to spontaneously generate sub-spinodal lengthscales remains a persistent pursuit. Elsewhere, thin liquid films experiments remain an invaluable probe to understand behavior of liquids in confinement [12]. Though a reconciliation of dewetting experiments with theory and simulations in terms of forces, length and time scales and morphology has already happened [13–15], recent reports about reduced viscosity in thinner polymer films [16, 17], necessitate a recalibration. The reason for this anisotropic viscosity as explained is twofold. Primarily it is considered that near-to-surface polymer chains in coil-size thick layers shows accelerated reptation due to reduced contact with a very thin molten region between them and the substrate. Secondly, exclusion of other chains due to reduced pervaded volume of the near-to-surface chains leads to lesser entanglement and allows for other modes of movements in addition to reptation thereby decreasing the viscosity near the substrate. The present letter principally aims to show that this decrease in viscosity with decreasing thickness leads to emergence of sub-spinodal lengthscales through formation of satellite holes without invoking heterogeneous substrate or nucleation. Additionally, it shows that signatures of slipping films, faster rupture and flatter morphologies, are

also present in the early stages of dewetting of these non-slipping films. This makes interpretation of experiments with films such as polystyrene films even more complex as they are likely to exhibit slippage as well as variable viscosity. Though not expressly shown in the letter, due to constraints of prohibitively large simulations, the generation of multimodal distribution of lengthscales is a natural extension of its findings.

A liquid film spontaneously dewets an underlying substrate under the influence of favorable excess intermolecular forces if it is thinner than their effective range (~ 100 nm). The dewetting process can be thought of as a combination of (i) a pre-rupture stage or early stage which is before the formation of first dry spot or hole on the solid followed by (ii) a post-rupture stage where the holes grow laterally and interacts with neighbouring growing holes to trap long cylindrical liquid ribbons in between. These ribbons break up to form droplets which become spherical under the influence of interfacial tension. So the result of dewetting process is a collection of disjointed liquid droplets on the dewetted solid. [3, 18]. The simplest force field which allows to study dewetting is long range van der Waals attraction combined with much shorter range Born repulsion [18]. The excess intermolecular forces per unit area ϕ , related to the excess free energy ΔG per unit area via ($\phi = \frac{\partial \Delta G}{\partial h}$), is given by $\phi = -2S^{LW}(\frac{d_0^2}{h^3}) \left[1 - \left(\frac{l_0}{h}\right)^6 \right]$ for this force field. Here S^{LW} is the spreading coefficient of the film liquid on the substrate, d_0 is a cut-off distance (0.158 nm) and l_0 is chosen such that $\phi(l_0) = 0$ and $\Delta G(l_0) = S^{LW}$. We consider the thickness dependent viscosity, μ , to be given by $\mu(h) = \mu_b + (\mu_f - \mu_b)(1 - e^{-((h-l_0)/b)^\beta})$ which is similar to the form reported in the experimental findings [17]. Here μ_f is the bulk viscosity obtained as $h \rightarrow \infty$ and μ_b is the base viscosity or the viscosity at the substrate obtained as $h \rightarrow l_0$, b is related to the radius of gyration and the constant β is taken as 6.8 in the simulations. Some representative variations in viscosity for a given bulk viscosity, μ_f , of $10^9 Pa.s$ are shown in fig. 1A. Nondimensional viscosity, $\eta = \mu/\mu_b$, is given by $\eta = 1 + (M-1)(1 - e^{-((H-L)/B)^\beta})$. Where H , L and B are the nondimensional thicknesses with respect to mean thickness h_0 and $M = \mu_f/\mu_b$ is the

* jayati@chemical.iitd.ac.in

† rajkh@chemical.iitd.ac.in

bulk to base viscosity ratio. Fig. 1A shows that higher value of M mean reduced viscosity at the substrate (μ_b) for the same bulk viscosity (μ_f). The evolution equation for the incompressible thin film with anisotropic viscosity effects obtained from Navier Stokes equations after long wave approximation and considering kinematic, shear free and capillary pressure boundary conditions at the free surface and no-slip and impermeability boundary conditions at the film-substrate interface is given by

$$3h_t + \vec{\nabla} \cdot [h^3 \vec{\nabla} (\gamma \nabla^2 h - \vec{\nabla} \phi) / \mu(h)] = 0 \quad (1)$$

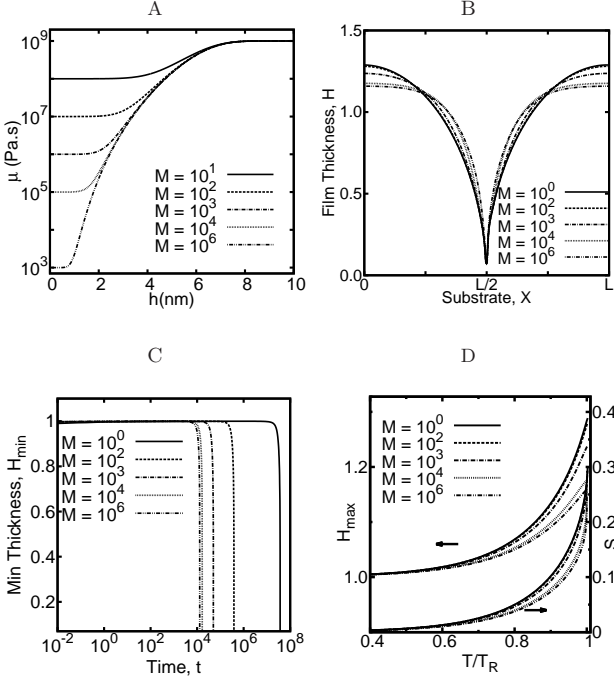


FIG. 1. (A) Variation of dimensional viscosity μ with film thickness h (B) Morphologies of films at rupture with thickness 2 nm and different film to base viscosity ratio M in a domain of size λ_m . (C) Steep decrease in values of H_{min} (D) Flatter profiles with lower values of H_{max} and S are found for films with high values of M .

The spinodal lengthscale or the dominant wavelength of the instability as given by linear stability analysis is the same as that of the constant viscosity films and is given as $\lambda_m = 2\pi \left(-\frac{2\gamma}{\phi_{h_0}} \right)^{1/2}$. Here ϕ_{h_0} is the spinodal parameter (derivative of ϕ) evaluated at $h = h_0$. The linear time of rupture marked by trough of the spinodal wavelength reaching the substrate in linear analysis is given as $t_r = \frac{\gamma \mu(h_0) h_0^5}{3(S^{LW} d_0^2 [1 - 3(\frac{t_0}{h_0})^6])^2} \ln(\frac{|h_0 - l_0|}{\epsilon})$. It is clear that films with reduced viscosity e.g., films less than about 6 nm in fig. 1A are expected to show a correspondingly reduced linear time of rupture. The nonlinear time of rupture will also be reduced as it is intimately related to

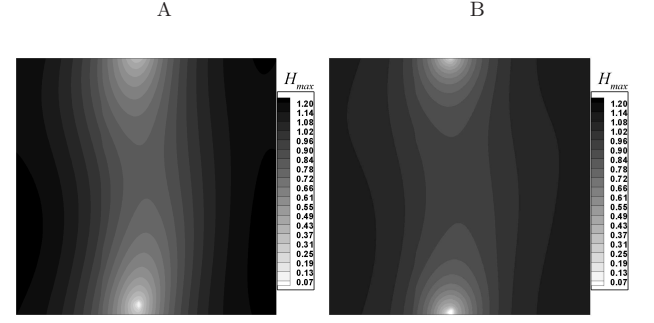


FIG. 2. 3D morphological patterns at rupture for 2 nm mean film thickness for (A) constant viscosity and (B) high value of viscosity ratio ($M = 10^6$) respectively.

the linear one [18]. Simulations were performed on 2D and 3D versions of the nondimensionalized form of the evolution equation

$$H_T + \vec{\nabla} \cdot [H^3 \vec{\nabla} (\nabla^2 H - \vec{\nabla} \Phi) / \eta[H]] = 0 \quad (2)$$

The non-dimensionalized parameters are given by $H = \frac{h}{h_0}$, $\vec{X} = \frac{1}{h_0} (\frac{d_0}{h_0}) (\frac{6|S^{LW}|}{\gamma})^{1/2} \vec{x}$, $T = (\frac{d_0}{h_0})^4 (\frac{12}{\mu_b \gamma h_0}) (|S^{LW}|)^2 t$ and $\Phi = \frac{1}{6|S^{LW}|} (\frac{h_0^3}{d_0^3}) \phi$ [18]. Simulations were carried out in $n \times \lambda_m$ sized linear and square domains ($n = 0.5, 1, 2, \dots$) by finite differencing in space using successive half-node central differencing and integration in time using NAG library's subroutine D02EJF. An ADI scheme was employed for 3D simulations. A grid density of 192 points per λ_m for 1 nm thick film was found to be satisfactory. Thicker films were simulated with a grid density varying as square of the film thickness appropos the nondimensionalization.

We first show that the early stages of dewetting carries signature of slipping films even though one is simulating non-slipping films. It is now established that the early stage of dewetting in slipping films are characterized by faster rupture, flatter morphologies around the growing depression and larger spinodal wavelengths [6, 7, 19–22]. Fig. 1B illustrates the surface morphology at the time of rupture of a 2 nm film as the viscosity ratios M increases from unity (constant viscosity case) to a high value of 10^6 . The film around the hole becomes progressively flatter as one increases the M by reducing the μ_b while keeping the same μ_f . This is due to the dispersal of lesser material into the surrounding film as the reduced viscosity at thinner regions dictates that lesser liquid needs to be scooped to form the hole. This is evidenced by the increasing sharpness of the hole profile as M increases. Also, faster hole formation as shown in fig. 1C means that the crest of the spinodal wave do not get a chance to develop fully before the hole forms. The evolution of surface morphology as marked by maximum non dimensional thickness, H_{max} , and root mean square surface roughness, S , also corroborate this (refer to Fig. 1D). Both evolve to a lesser extent indicating flatter morphology as M is increased.

The spinodal wavelength here remains unchanged from that of constant viscosity film. In slipping films the spinodal wave length increases considerably [6] and this fact can be exploited to differentiate between slipping films and films with variable viscosity. However, as the spinodal wavelength itself is a crucial input to the estimate of the often unknown excess intermolecular force field, one can not really know if it has increased or reduced. Same is the case with reduced time scales also [23]. The flatness of the surrounding film which remains free of these issues and can serve as a differentiating marker remains the same in both cases. The flatness of the surrounding film, though, is not easy to resolve in experiments. Even in simulations, it is not easy as shown in fig. 2 which presents the contour map of film's surface at the time of hole formation for constant viscosity film and a film having very high value of M . If one observes closely, one can see more contours in between the holes for Fig. 2A indicating different depths of the film surface. Where as for higher M (Fig. 2B) the lesser number of contours in between the depression demonstrate a sharper hole profiles with flatter surroundings.

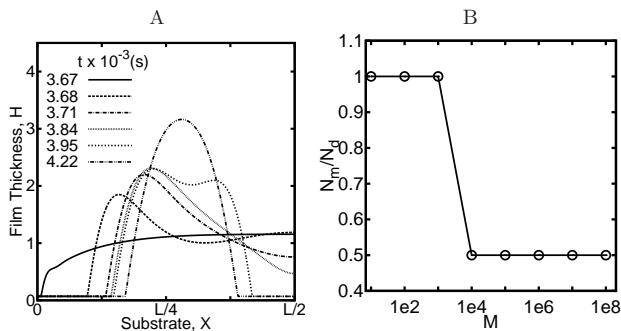


FIG. 3. Hole growth phase after rupture. (A) Hole growth for a film of thickness 2 nm simulated in a domain of size $\lambda_m/2$ with viscosity ratio $M = 10^6$. Kinetics of the film helps in formation of satellite hole. (B) Effect of M on the ratio of lengthscales formed at equilibrium to that predicted by linear stability analysis for films of thickness 2 nm in a domain of size $2\lambda_m$.

We now show the emergence of sub-spinodal length-scale in the later stages of dewetting. Fig. 3 presents the results for post-rupture variations in morphology of a 2 nm film with a very high viscosity ratio of 10^6 . The simulations are done in one-half of the spinodal wavelength for faster simulations as well as better spatial resolution. Symmetry boundary conditions at both ends were used to have zero liquid flux at the edges. These were preferred to usual periodic boundary conditions which are relevant whenever simulations are done in integral multiples of spinodal wavelengths. The hole grows as reported extensively in the past [3, 18] and mismatch between the rate of dewetting and subsequent dispersal on the surrounding film forms an asymmetric elevated

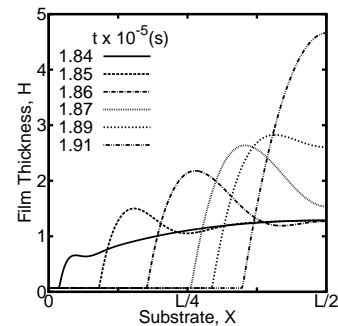


FIG. 4. Hole growth phase after rupture. Hole growth for a film of thickness 2 nm simulated in a domain of size $\lambda_m/2$ with viscosity ratio $M = 10$.

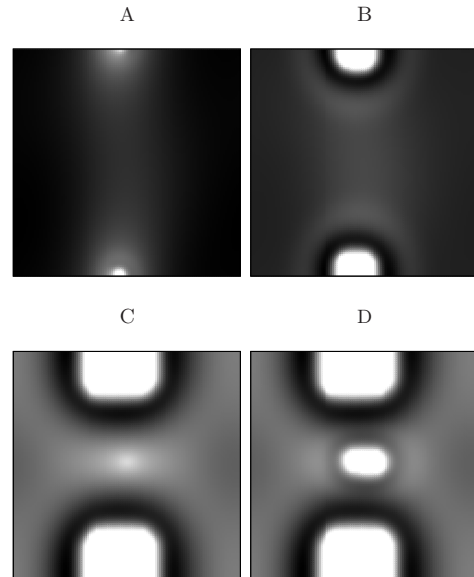


FIG. 5. 3D morphological evolutions for film of thickness 2 nm and viscosity ratio $M = 10^6$ undergoing satellite hole formation. The dimensional time associated with the different stages of evolution are A)1012 s, B)1012.73 s, C)1024.49 s, D)1025.88 s respectively.

rim at the hole edge with a depression on the far side ($t = 3.68 \times 10^3$ s). The further part of the film shows no effect. Soon, the depression reaches the end of the domain and the growing hole starts interacting with the neighbouring hole (not shown). At this point the depression deepens further to form a satellite hole ($t = 3.84 \times 10^3$ s, 3.95×10^3 s, 4.22×10^3 s) which also starts growing. The liquid trapped between the satellite hole and the primary hole becomes increasingly circular under the influence of interfacial tension and forms a droplet. Thus, one full droplet emerges in only one-half of the spinodal wavelength making two droplets per spinodal wavelength. Large domain simulations with periodic boundary conditions (morphologies not shown here) also confirm the formation of satellite holes and subsequent increase in the number of droplets per spinodal wavelength. In complete

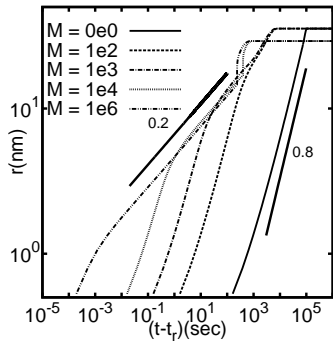


FIG. 6. Dewetted length (r) at different times after rupture for a film of thickness 2 nm simulated in a domain of size $\lambda_m/2$ for different viscosity ratios M . The bold lines are the slopes and hence indicative of the growth law exponents (α) for different M .

contrast to this, films with lesser viscosity ratio follow the normal dewetting process. Both these effects can be seen from Fig. 3B which shows that for smaller M values the number of holes formed (N_d) is the same as predicted by linear stability analysis (N_m). However, the ratio N_m/N_d is much smaller for higher value of M indicating sub-spinodal lengthscales due to formation of satellite holes. Fig. 4 presents results for $M = 10$ where the depression at the far end of the rim does not deepen to form a satellite hole but rises up to form a liquid ribbon between two growing primary holes ($t = 1.91 \times 10^5$ s). In this case the depression gets filled up due to pouring of the liquid from the rims of the growing primary neighbouring holes before it can thin under the influence of excess intermolecular forces. This influx of liquid into the intervening depression is not possible for high values of M due to higher viscosity at the rims and lower viscosity at the depression. This combined with the ability of forming sharper holes (Fig. 1) by removal of lesser material manifests into formation of satellite holes for these films. Formation of satellite holes is confirmed by 3D simulations also. Simulations were carried out in a unit

cell of spinodal wavelength side with periodic boundary conditions for the same 2 nm thick film. Fig. 5 which shows grayscale map of the surface morphology of the film shows deepening of the intervening depression into a satellite hole between two growing primary holes.

The rate of dewetting can be given by growth law $r \propto t^\alpha$ where r is the dewetted length. Fig. 6 represents the growth of dewetted length in 2D simulations which has contributions from both primary and satellite holes (if and when formed). For constant viscosity case it is well known that the exponent α has much higher values of 0.8 and above [18, 24] as also seen from Fig. 6. However, films with higher M the exponent has a much lower value (~ 0.2) for $M = 10^6$. Thus, even the growth law shares the tendency of slipping films to have lower exponents. However, the exponents for slipping films decrease to about 2/3 only [12]. Previous studies of dewetting of non-Newtonian thin films with shear thinning or shear thickening effects have shown to display only change in rupture times without any change in length-scales [23]. For the first time it is shown in this letter that viscosity decreasing with decreasing film thickness leads to nonlinear mobility factor which now has a non-cubic variation with thickness and has important effects on the thin film instability. Based on the simulations it is clear that these non-slipping, viscosity varying films on homogeneous substrate show sharper holes, flatter morphologies, faster rupture at pre-rupture stage like slipping films. Post rupture these films lead to formation of satellite holes giving rise to sub-spinodal length scales which so far was considered to be only possible for films dewetting on heterogeneous substrates or undergoing nucleation. Thus, if one uses the dewetting of thin films as a cantilever to understand the underlying force field in case of films with anisotropic viscous effects is bound to miscalculate the force field and would consider it to be much stronger than it really is if the graded viscosity effect is neglected. On the other hand this retarded viscosity effect can be beneficially utilized to fabricate miniaturized patterns.

-
- [1] E. Ruckenstein and R. K. Jain, Faraday Trans. **70**, 132 (1974)
 - [2] F. Brochard-Wyart and J. Daillant, Can. J. Phys. **68**, 1084 (1990)
 - [3] G. Reiter, Phys. Rev. Lett. **68**, 75 (1992)
 - [4] G. Reiter, R. Khanna, and A. Sharma, Phys. Rev. Lett. **85**, 1432 (2000)
 - [5] B. Liu, Y. Yao, and S. Che, Angew. Chem. Int. Ed **52**, 14186 (2013)
 - [6] K. Kargupta, A. Sharma, and R. Khanna, Langmuir **20**, 244 (2004)
 - [7] R. Fetzer, K. Jacobs, A. Munch, B. Wagner, and T. P. Witelski, Phys. Rev. Lett. **95**, 127801 (2005)
 - [8] A. Sharma and J. Mittal, Phys. Rev. Lett **89**, 186101 (2002)
 - [9] J. Sarkar and A. Sharma, Langmuir **26**(11), 8464 (2010)
 - [10] K. Jacobs, R. Seemann, and K. Mecke, springer verlag berlin heidelberg **554**, 372 (2000)
 - [11] R. Konnur, K. Kargupta, and A. Sharma, Phys. Rev. Lett. **84**, 931(4) (2000)
 - [12] G. Reiter, Adv. Polym. Sci. **252**, 29 (2013)
 - [13] A. Sharma and R. Khanna, Phys. Rev. Lett. **81**, 3463 (1998)
 - [14] S. Herminghaus, K. Jacobs, K. Mecke, J. Bischof, A. Fery, M. Ibn-Elhaj, and S. Schlagowski, Science **282**, 916 (1998)
 - [15] G. Tomar, V. Shankar, S. K. Shukla, A. Sharma, and G. Biswas, Euro. Phys. J. E. **20**, 185 (2006)
 - [16] J. L. Masson and P. F. Green, Phys. Rev. E. **65**, 031806 (2002)

- [17] H. Bodiguel and C. Fretigny, Phys. Rev. Lett. **97**, 266105 (2006)
- [18] R. Khanna and A. Sharma, J. Coll. and Int. Sci. **195**, 42 (1997)
- [19] G. Reiter, Macromolecules **27**, 3046 (1994)
- [20] A. Sharma and R. Khanna, Macromolecules **29**, 6959 (1996)
- [21] G. Reiter and R. Khanna, Phys. Rev. Lett. **85**, 2753 (2000)
- [22] R. Fetzer and K. Jacobs, Langmuir **23**, 11617 (2007)
- [23] A. Sharma, Eur. Phys. J. E **12**, 397 (2003)
- [24] A. Ghatak, R. Khanna, and A. Sharma, J. Coll. and Int. Sci. **212**, 483 (1999)